

3D HYBRID MESH GENERATION FOR RESERVOIR FLOW SIMULATION

N. Flandrin¹

H. Borouchaki²

C. Bennis¹

¹*Institut Français du Pétrole, 1 & 4 avenue de Bois Préau, 92852 Rueil-Malmaison Cedex, France.
nicolas.flandrin@ifp.fr and chakib.bennis@ifp.fr*

²*Université de Technologie de Troyes, 12 rue Marie Curie, BP 2060, 10010 Troyes Cedex, France.
houman.borouchaki@utt.fr*

ABSTRACT

A great challenge for flow simulators of new generation is to gain more accuracy at well proximity within complex geological structures. For this purpose, a new approach based on hybrid mesh modeling was proposed in 2D in [1]. In this hybrid mesh, the reservoir is described by a structured quadrilateral mesh and drainage areas around wells are represented by radial circular meshes. In order to generate a global conforming mesh, unstructured transition meshes constituted by convex polygonal elements satisfying finite volume properties are used to connect together these two structured meshes. Thus, the resulting mesh allows us to take full advantages of simplicity and practical aspects of structured meshes while complexity inherent to unstructured meshes is introduced only where strictly needed.

This paper presents the 3D extension of the generation of such a hybrid mesh [2]. The proposed method uses 3D power diagrams to generate the transition mesh. Due to the round off errors, this mesh is modified in order to ensure the conformity with the structured meshes. In addition, some criteria are introduced to measure the mesh quality, as well as an optimization procedure to remove and to expand small edges of the transition mesh under finite volume properties constraints. Numerical results are given to show the efficiency of the approach.

Keywords: computational geometry, hybrid mesh, power diagram, Delaunay and regular triangulations

1. INTRODUCTION

Nowadays, the new technological progress in 3D seismic imagery and drilling/production permits to obtain a realistic and faithful image of the internal architecture of the reservoir and to drill deviated and complex 3D wells with several levels of ramification. Nowadays well trajectories can be well adapted to the geometry of the reservoir in order to optimize its production. In this new technological context, the mesh generation becomes a crucial step in the reservoir flow simulation of new generation. Meshes allow us to describe the geometry of the geological structure with a representation in discrete elements on which the simulation is processed. A better comprehension of the physical phenomena requires us to simulate 3D multiphase flows in increasingly complex geological structures, in

the vicinity of several types of singularities such as complex wells. All these complexities must be initially taken into account within the mesh construction. The mesh must faithfully represent all this heterogeneous information.

The current industrial standard meshes, based on Corner Point Geometry (CPG) grids already showed their limits. They are very practical and easy to use, but they fail to represent complex objects due to their structured aspect. More recently, other approaches have been proposed in particular the PErpendicular BIssector (PEBI) grids which are completely unstructured. They are obtained using Voronoi diagrams that are derived from Delaunay triangulations. These grids are very flexible and can model most complex shapes. But, they are often difficult to use and to understand

in 3D, because they are difficult to visualize and to explore from the inside, due to their lack of structure. In [3], a new hybrid mesh model was proposed in 2D to capture the radial characteristics of the flow around the wells. It combines the advantages of the structured and unstructured approaches, while limiting their disadvantages. The hybrid mesh is composed of a structured quadrilateral mesh describing the reservoir field, structured radial meshes adapted locally to flow directions around each well and unstructured polygonal meshes (based on power diagrams) connecting together the two structured meshes.

In this paper, the generation of the hybrid mesh is extended in 3D. In Section 2, we present the numerical constraints imposed by finite volume schemes that will govern the mesh construction. Section 3 recalls the methodology used to generate a hybrid mesh in 2D. In Section 4, we describe briefly some known facts related to Delaunay and regular triangulations. Section 5 is devoted to the 3D extension of such a hybrid mesh taking into account mesh conformity problems. In Section 6, three criteria to measure the mesh quality as well as an optimization procedure based on these criteria are introduced. In Section 7, some numerical results are given.

2. STATEMENT OF THE PROBLEM

The proposed hybrid mesh model is composed of a structured CPG grid, respecting the geological features to describe the reservoir field, a structured radial circular mesh adapted locally to the radial nature of the flows around the wells to gain accuracy at the drainage areas and an unstructured polyhedral mesh preserving finite volume properties to connect together the above structured meshes.

While the structured grid generation is a well known process, the construction of the unstructured transition mesh in 3D represents a major issue. The structured CPG mesh of the reservoir grid is constructed through the use of transfinite interpolations, projections onto the geological interfaces (horizons and faults) combined by a relaxation procedure [4]. The structured radial mesh is computed by using the well's trajectory, the drainage area radius and the progression of cells' size. The separate construction of these grids leads to incompatibilities due to a lack of common structure and a transition mesh is needed to perform a correct connection. For accurate simulation purposes, the transition mesh must verify the following numerical requirements:

- convexity: each polyhedral element (cell) is convex,
- conformity: any two adjacent cells share a unique

face,

- dual orthogonality: the line joining the centers of two adjacent cells is orthogonal to the shared face,
- auto-centering: the site (or center) of each cell lies inside the cell.

In order to generate such a transition mesh, a new method using *power diagrams* [5, 6] was introduced in [1]. As a generalization of Voronoi diagrams [7, 8], power diagrams provide convex polyhedra verifying the above orthogonal property. In addition, these allow here to reach the mesh conformity between the transition mesh and structured meshes which would not be generally possible using Voronoi diagrams. The goal of this work is to extend the construction of the transition mesh based on power diagrams into 3D.

3. METHODOLOGY IN 2D

Given a reservoir mesh, a well mesh is first introduced at a specific position (Figure 1 on the left). The two meshes are then superimposed and a cavity between the well and the reservoir is defined by deactivating certain cells of the reservoir (Figure 1 on the right). These cells cut well mesh elements or contain an edge with a diametral circle containing a well mesh vertex or contain a vertex belonging to the diametral circle of a well mesh edge. Finally, the boundary edges of the cavity (which constitute the boundary of the transition mesh) are extracted. The problem is now to construct a power diagram whose cells exactly fit the cavity and whose external edges correspond to the edges of the cavity boundary (the constrained edges).

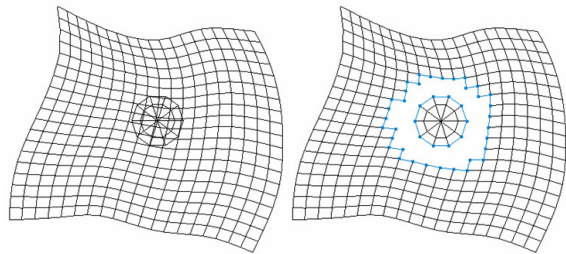


Figure 1: Definition of a cavity between the well and the reservoir.

The construction scheme is the following:

- The Delaunay triangulation¹ of the cavity vertices is generated (Figure 2 on the left). All cavity edges belong to the triangulation (*Delaunay*

¹The Delaunay triangulation of a set S of points in \mathcal{R}^d ($d = 2$ or 3) is such that the open circumballs of its simplices contain no point of S .

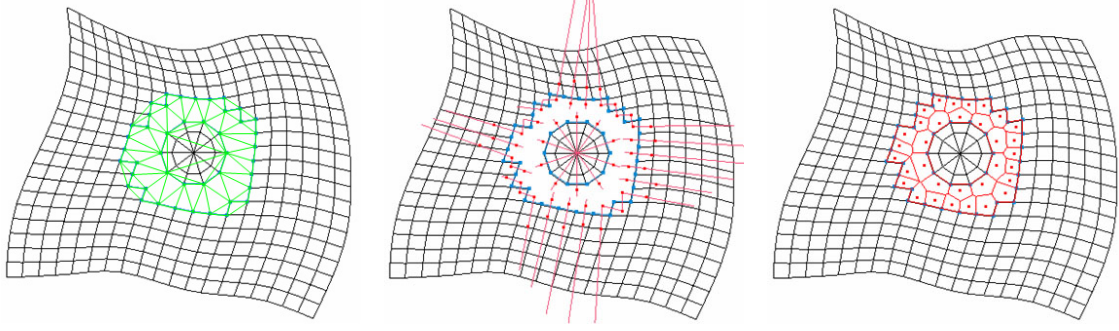


Figure 2: Determination of the weighted points of the cavity and construction of the corresponding power diagram.

admissibility property) as their diametral circles are empty.

- For each constrained edge e of the cavity, two weighted points (P_1, ω_1) and (P_2, ω_2) are determined on the Voronoi edge associated with e , one inside the cavity and the other outside of the cavity (Figure 2 in the middle).
- Finally, the power diagram having as sites the internal weighted points of the cavity is generated (Figure 2 on the right). This diagram is the expected transition mesh.

4. DELAUNAY AND REGULAR TRIANGULATIONS

4.1 Delaunay triangulation

The Delaunay triangulation can be introduced in various ways (according to the context of the application). One of those is to use its dual: the Voronoi diagram.

Let $\mathcal{S} = \{P_1, \dots, P_n\}$ be a set of points in \mathcal{R}^3 . The Voronoi diagram of \mathcal{S} is the set of cells V_i defined by:

$$V_i = \{P \in \mathcal{R}^3 \mid \|\overrightarrow{PP_i}\| \leq \|\overrightarrow{PP_j}\|, \forall j \neq i\} \quad (1)$$

Each cell corresponds to a point P_i of \mathcal{S} and is the set of its closest points in \mathcal{R}^3 with respect to other points of \mathcal{S} .

From the Voronoi cells of \mathcal{S} , the dual can be constructed in order to give the expected Delaunay triangulation. In particular, faces of Voronoi cells, which are equidistant from the two points they separate, define the mediating planes of the edges of the triangulation. In other words, the expected triangulation is obtained (or more exactly the edges of this one) by joining vertices of \mathcal{S} which belong to two adjacent cells. When points of \mathcal{S} are in general position²,

²A set of points is said to be in general position when there is no configuration of more than four cocyclical points.

the obtained triangulation is unique and is composed of tetrahedra. Otherwise, non-simplicial elements are constructed; they can subsequently be subdivided into tetrahedra (giving rise to more than one triangulation for the same set of points).

4.2 Regular triangulation

Weighted point: Let P be a point in \mathcal{R}^3 and let ω be a scalar called the weight of point P . The weighted point (P, ω) is the sphere of center P and radius ω .

Power: The power of a point X with respect to a weighted point (P, ω) is given by:

$$\Pi(X, (P, \omega)) = \|\overrightarrow{PX}\|^2 - \omega^2 \quad (2)$$

Power product: The power product of two weighted points (P_i, ω_i) and (P_j, ω_j) is defined by:

$$\Pi((P_i, \omega_i), (P_j, \omega_j)) = \|\overrightarrow{P_i P_j}\|^2 - \omega_i^2 - \omega_j^2 \quad (3)$$

Notice that if the weight ω_i is equal to zero, the power product $\Pi((P_i, \omega_i), (P_j, \omega_j)) = \Pi(P_i, (P_j, \omega_j))$ is the power of the point P_i with respect to the weighted point (P_j, ω_j) .

The weighted points (P_i, ω_i) and (P_j, ω_j) are said to be orthogonal if their power product is equal to zero.

Radical plane: The radical plane of two weighted points (P_i, ω_i) and (P_j, ω_j) is the locus of points in \mathcal{R}^3 whose power with respect to (P_i, ω_i) is equal to its power with respect to (P_j, ω_j) .

Power sphere: The power sphere of four weighted points (P_i, ω_i) , (P_j, ω_j) , (P_k, ω_k) and (P_l, ω_l) is the unique sphere (P, ω) which is orthogonal to each of these weighted points.

Power diagram: Let $\mathcal{SW} = \{(P_1, \omega_1), \dots, (P_n, \omega_n)\}$ be a set of weighted points where each P_i is a point in \mathcal{R}^3 and each ω_i is the weight of point P_i . The power

diagram of \mathcal{S} is the set of cells V_i defined by:

$$V_i = \{X \in \mathcal{R}^3 \mid \Pi((P_i, \omega_i), X) \leq \Pi((P_j, \omega_j), X), \quad \forall (P_j, \omega_j) \in \mathcal{SW}, j \neq i\} \quad (4)$$

Each cell corresponds to a weighted point (P_i, ω_i) of \mathcal{SW} and is the locus of points P in \mathcal{R}^3 whose power with respect to (P_i, ω_i) is less than its power with respect to any other weighted point (P_j, ω_j) of \mathcal{SW} . The power diagram extends the notion of Voronoï diagram in the sense that a Voronoï diagram is a power diagram of equally weighted points. Notice, however, that a weighted point can have no cell (or more exactly an empty cell) in the power diagram of \mathcal{SW} .

Regular triangulation: From the power cells of \mathcal{SW} , the dual can be constructed in order to give the expected regular triangulation. In particular, faces of power cells, which have an equal power with respect to the two weighted points they separate, define the radical planes of the edges of the triangulation. In other words, the expected triangulation is obtained (or more exactly the edges of this one) by joining vertices of \mathcal{SW} which belong to two adjacent cells (Figure 3). When weighted points of \mathcal{SW} are in general position³, the obtained triangulation is unique and is composed of tetrahedra. Otherwise, non-simplicial elements are constructed; they can subsequently be subdivided into tetrahedra (giving rise to more than one triangulation for the same set of points).

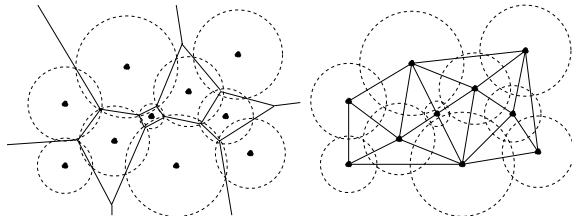


Figure 3: Power diagram (on the left) and the corresponding regular triangulation (on the right).

The regular triangulation extends the notion of Delaunay triangulation since a Delaunay triangulation is a regular triangulation whose weights are all equal.

4.3 Construction scheme

Delaunay and regular triangulations can be constructed in various manners (for example, from their duality with Voronoï and power diagrams). Among the whole of existing methods, the *incremental method* (also known under the name of Watson algorithm [9])

³A set of weighted points is said to be in general position when there is no configuration of more than four weighted points having an equal power with respect to the same point $X \in \mathcal{R}^3$.

seems to be the best adapted to our problem as it can also be applied to the regular triangulation [10].

The following results are established for the Delaunay triangulation but remain valid for the regular triangulation by replacing the circumscribed spheres of the tetrahedra by their power spheres.

Incremental method: Let \mathcal{S} be a set of points in \mathcal{R}^3 . Let \mathcal{T}_i be the Delaunay triangulation of the convex envelope of the first i points of \mathcal{S} and let P be the $(i + 1)^{th}$ point of this set.

The goal of the incremental method is to construct \mathcal{T}_{i+1} , the Delaunay triangulation of the first $(i + 1)$ points of \mathcal{S} , from the triangulation \mathcal{T}_i , such that P is vertex of elements. For this purpose, the *Delaunay kernel* is introduced as follows [11]:

$$\mathcal{T}_{i+1} = \mathcal{T}_i - \mathcal{C}_P + \mathcal{B}_P \quad (5)$$

where \mathcal{C}_P is the polytope constituted by tetrahedra whose circumballs contain point P and \mathcal{B}_P is the set of tetrahedra formed by joining P to the external faces of \mathcal{C}_P .

From a practical point of view, the significant and directly usable result is that the cavity is a star-shaped polytope with respect to the point P .

5. CONSTRUCTION OF THE TRANSITION MESH IN 3D

In 3D, the generation of the hybrid mesh is extended to reservoirs described by non-uniform cartesian grids. The problem is first to define a cavity which is Delaunay admissible and then to construct a 3D power diagram whose external faces fit exactly the constrained quadrilaterals constituting the cavity boundary.

5.1 Cavity definition

In order to obtain a cavity whose faces belong to tetrahedra of the Delaunay triangulation of the cavity vertices, the *Gabriel condition* could be verified by the well and the reservoir meshes. This condition (which is a strong condition ensuring the Delaunay admissibility) can be defined as follows: Let E_c be a set of vertices and edges, an edge of E_c is said to be Gabriel if its diametral sphere contains no points of E_c .

The edges of the cartesian hexahedral mesh of the reservoir satisfy the Gabriel condition. This implies that the facets of the reservoir mesh are Delaunay admissible.

On the other hand, the well mesh is not necessarily Gabriel (Figure 4 on the left). In particular, in certain configurations, some edges, located on the extremities of the well, do not satisfy the empty diametral sphere

property. In this case, the well mesh is not Gabriel and some of its facets may not appear in the Delaunay triangulation of its vertices. Such a well can however be modified in order to become Gabriel. Actually, the number of well subdivisions can be increased in the θ direction (Figure 4) or segments of a sphere can be added, one on each extremity of the well (Figure 5).

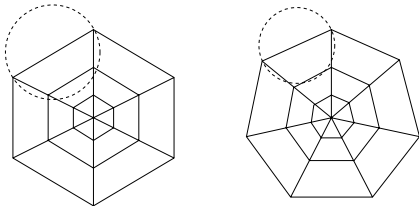


Figure 4: Non-Gabriel well mesh (on the left) and Gabriel well mesh (on the right).

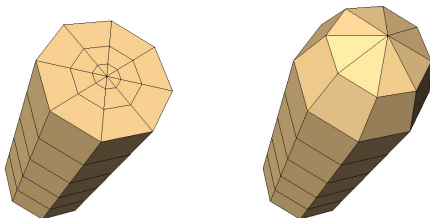


Figure 5: Well mesh without and with a segment of a sphere.

Therefore, the cavity is said to be Gabriel and so Delaunay admissible if the diametral sphere of each edge of the reservoir contains no point of the well and if the diametral sphere of each edge of the well contains no point of the reservoir.

In order to define a Delaunay admissible cavity that makes it possible to generate a transition mesh whose size is intermediate between the mesh size of the well and the reservoir, a local coefficient of expansion α (depending on the local mesh size of the well and the reservoir) is introduced and the well is dilated according to this coefficient. Cells of the reservoir intersecting the image of the dilated well are then deactivated (Figure 6). The boundary of the cavity is extracted. It consists of constrained quadrilaterals which are the limit of the transition mesh to construct.

5.2 Delaunay triangulation of the cavity vertices

In order to determine the *Voronoi edges* of the cavity quadrilaterals (as the quadrilateral faces have four co-circular vertices), a Delaunay triangulation of the

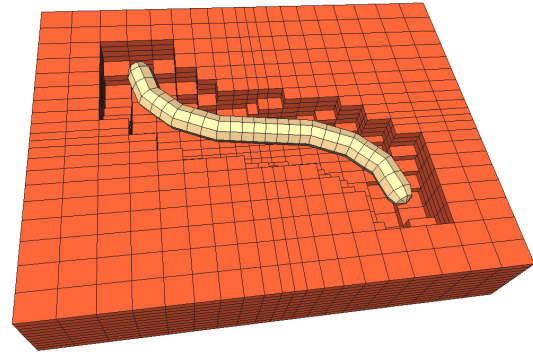


Figure 6: Cavity definition between the well and the reservoir meshes.

bounding box of the cavity vertices is generated using an incremental method [11, 12].

5.3 Search of the tetrahedra attached to the boundary cavity quadrilaterals

Since the cavity is Delaunay admissible, constrained quadrilaterals of the cavity are shared by tetrahedra of the Delaunay triangulation of the cavity vertices (at most four, two inside and two outside of the cavity). In particular, the constrained quadrilaterals of the cavity are subdivided into two triangles and these triangles are facets of tetrahedra of the triangulation.

Let Q be a quadrilateral defined by vertices A , B , C and D . The four tetrahedra T_{1in} , T_{2in} , T_{1out} and T_{2out} which are attached to the quadrilateral Q and which are respectively inside (*in*) and outside (*out*) of the cavity, are found using the following process:

1. Explore the ball⁴ of vertex A to find a tetrahedron T_0 shared by the edge $[AB]$.
2. Explore the shell⁵ of edge $[AB]$ to find a tetrahedron T_1 shared by the triangular face (A, B, C) or (A, B, D) . Let f be this triangular face, let e_A be the edge of f opposite to vertex A and let i be the vertex of the tetrahedron T_1 such that $i \notin f$.
3. If i is also a vertex of the quadrilateral Q , the considered tetrahedron is a *sliver*⁶. In this case, the four required tetrahedra are the four neighboring tetrahedra of T_1 : two of them are inside

⁴Let P be a vertex of a mesh, the ball associated to P is the set of elements having P as vertex.

⁵Let e be an edge of a mesh, the shell associated to e is the set of elements having e as edge.

⁶A sliver is a tetrahedron having a volume practically null formed by 4 co-circular vertices.

the cavity and the two others are outside of the cavity.

4. Else, T_1 is one of the required tetrahedra: if T_1 is inside the cavity then $T_{1in} = T_1$ else $T_{1out} = T_1$. The search of the tetrahedron T_2 adjacent to T_1 and opposite to vertex i allows us to determine the complementary tetrahedron:
 - (a) If T_2 is a sliver, the required tetrahedra are the four neighboring tetrahedra of T_2 .
 - (b) Else, if T_1 is inside the cavity then $T_{1out} = T_2$ else $T_{1in} = T_2$.
5. If 4.(b), explore the shell of edge e_A to find a tetrahedron T_3 having the fourth vertex of Q as vertex.
6. If T_3 is a sliver, the required tetrahedra are the four neighboring tetrahedra of T_3 .
7. Else, the tetrahedron T_3 is one of the required tetrahedra: if T_3 is inside the cavity then $T_{2in} = T_3$ else $T_{2out} = T_3$. The search of the tetrahedron T_4 adjacent to T_3 allows us to determine the complementary tetrahedron:
 - (a) If T_4 is a sliver, the required tetrahedra are the four neighboring tetrahedra of T_3 .
 - (b) Else, if T_3 is inside the cavity then $T_{2out} = T_4$ else $T_{2in} = T_4$.

Figure 7 illustrates the different stages of the algorithm which permit to find the two tetrahedra attached to the face (A, B, C) of the quadrilateral Q .

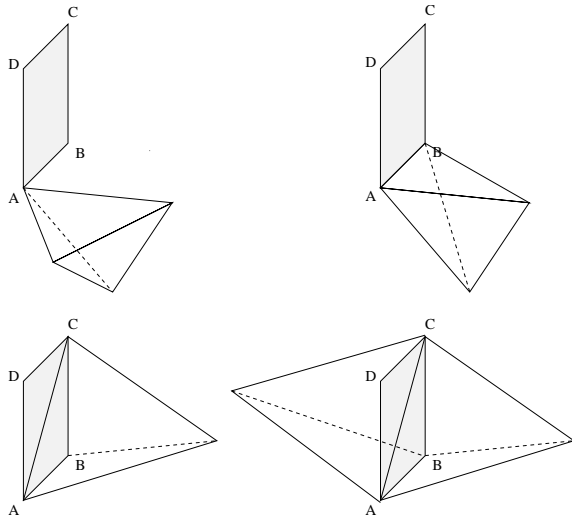


Figure 7: Search of the two tetrahedra sharing the face (A, B, C) (stages 1., 2. and 4.(b)).

5.4 Cavity sites definition

Tetrahedra attached to each constrained quadrilateral of the cavity (as defined above) allow us to define the Voronoï edges associated to the cavity quadrilaterals and thus to determine the cavity sites. In the general case, for each constrained quadrilateral, two sites are defined along its Voronoï edge, one inside and one outside of the cavity. When Voronoï edges of several quadrilaterals are intersecting, only one site is determined for all of these quadrilaterals. In particular, it happens when several quadrilaterals of the cavity belong to the same (inactive for internal sites or active for external sites) reservoir cell.

5.4.1 Internal sites definition

Let (P, ω) be an internal site of the cavity and let $\mathcal{Q} = \{Q_1, \dots, Q_n\}$ be the set of constrained quadrilaterals associated with this site. The Voronoï site V associated with the quadrilaterals of \mathcal{Q} is the barycenter of the circumcenters $\{O_1, \dots, O_{n_t}\}$ of the n_t internal tetrahedra attached to the quadrilaterals of \mathcal{Q} . The spatial coordinates of (P, ω) depend on the number of quadrilaterals n associated with the site. If $n > 1$, P is equal to V which is the only point of intersection of the dual edges of the quadrilaterals of \mathcal{Q} (Figure 8 on the left). Otherwise, P is obtained by calculating the midpoint of the segment $[OV]$ where O is the *circumcenter of the quadrilateral* Q_1 (this point is well defined as the vertices of the quadrilateral are co-circular). Actually, this position gives good results (Figure 8 on the right).

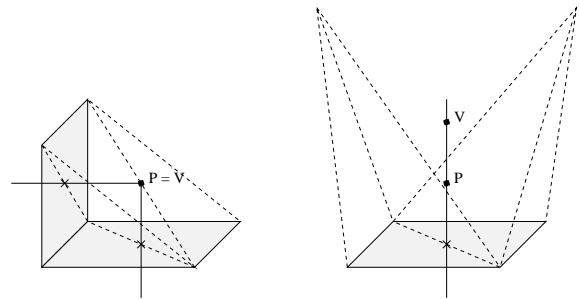


Figure 8: Position of the sites when $n = 2$ (on the left) and when $n = 1$ (on the right).

The weight ω (Figure 9) is the radius of the sphere of center P passing through its n_c constrained vertices $\{A_1, \dots, A_{n_c}\}$ ($4 \leq n_c \leq 8$). Thus, if the constrained quadrilaterals associated with (P, ω) are co-circular, P is exactly equidistant from its constrained vertices; the weight ω is then defined in an exact way by calculating the distance between P and one of its constrained vertices, for example A_1 . On the other hand, if the constrained quadrilaterals associated with (P, ω) are not co-circular, the weight ω is approximated by the

average distance between P and its n_c constrained vertices. In this case, problems of mesh conformity can occur (see 5.7).

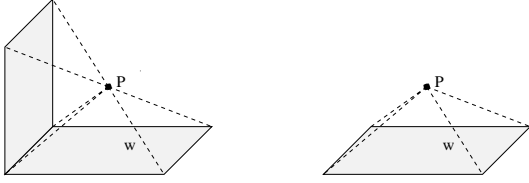


Figure 9: Weight ω of the sites.

5.4.2 External sites definition

The method used to determine the external sites of the cavity is somewhat different from the method described previously. Indeed, if the number n of quadrilaterals associated with the site is equal to one, this quadrilateral can be on the convex envelope of the cavity. In this case, there is no external tetrahedra (of the Delaunay triangulation) attached to the quadrilateral. The external site (P, ω) is then obtained by symmetry of the internal site (P', ω) with respect to the circumcenter O of the quadrilateral. In all the other situations (when $n > 1$), the method described in 5.4.1 remains valid.

5.5 Cavity sites validation

At this stage, a set of internal and external cavity sites has been defined. They guarantee the existence of a 3D power diagram which is orthogonal and which is in conformity with the constrained quadrilaterals of the cavity (if however the vertices of those quadrilaterals are co-circular and coplanar). Unfortunately, since the cavity sites are defined in an independent way, some empty or non auto-centered power cells may occur. In order to prevent such a thing, the mutual interaction between the cavity sites must be taken into account. A *correction procedure* modifying the position of certain sites via the correction of their weight, is thus proposed.

5.5.1 Auto-centering condition

Let (P_i, ω_i) and (P_j, ω_j) be two sites and let Γ_{ij} be their radical plane, i.e. the locus of points having equal power with respect to (P_i, ω_i) and (P_j, ω_j) . The power cells associated with (P_i, ω_i) and (P_j, ω_j) are auto-centered if these two sites are on both sides of Γ_{ij} . The necessary and sufficient condition for the radical plane Γ_{ij} cuts the segment $[P_i P_j]$ is:

$$|\omega_i^2 - \omega_j^2| \leq \|\overrightarrow{P_i P_j}\|^2 \quad (6)$$

5.5.2 Sites adjustment

Let (P_i, ω_i) and (P_j, ω_j) be two sites and let Γ_{ij} be their radical plane such that $|\omega_i^2 - \omega_j^2| > \|\overrightarrow{P_i P_j}\|^2$, i.e. such that the sites are located on the same side of Γ_{ij} . The site located outside of its cell is found inside if the radical plane Γ_{ij} is moved until being between (P_i, ω_i) and (P_j, ω_j) . Two solutions are possible. The first consists in modifying the weight of one of the sites, i.e. the radius of the sphere associated with the considered site (Figure 10). The second simply consists in moving one of the sites. This modifies the position of the intersection of the spheres associated with the sites and thus the position of the radical plane. However, in our case, the weight of a site is related to its position (the weight ω , associated with the point P , is equal to the average distance between P and the constrained vertices associated with the site). Thus, the weight cannot be modified without moving the site, and the site cannot be moved without modifying the weight. A combination of the two above process is then necessary. Actually, the site, whose weight is maximum, is moved along its Voronoï edge by bringing it closer to its constrained quadrilateral until the condition (6) is satisfied (Figure 11).

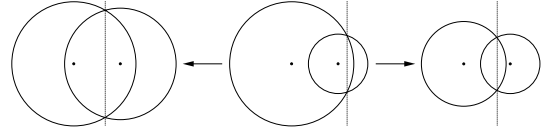


Figure 10: Weight modification of one of the sites.

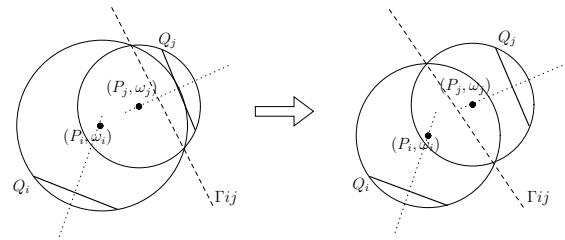


Figure 11: Moving a site via the correction of its weight.

5.5.3 Correction algorithm

The correction algorithm checks the condition (6) for all of the sites and modifies them if required. The cavity sites are corrected as follows:

1. Initialize the correction number n to zero.
2. For each site of the cavity (P_i, ω_i) , find the set of sites (P_j, ω_j) , $j \neq i$ such that $\|\overrightarrow{P_i P_j}\|^2 \leq \omega_i^2$. For

all pair $((P_i, \omega_i), (P_j, \omega_j))$, evaluate the difference $|\omega_i^2 - \omega_j^2|$. If it is greater than $\|\overrightarrow{P_i P_j}\|^2$, increment n . If (P, ω) is the site whose weight is maximum, move P along its Voronoï edge by bringing it closer to its constrained quadrilateral. In particular, if O is the circumcenter of the quadrilateral associated with (P, ω) , $P = O + \alpha \overrightarrow{OP}$ ($0.7 \leq \alpha < 1$) and ω is updated by the same occasion.

3. If $n > 0$, go to 1.

The new spatial configuration of the cavity sites satisfies the finite volume properties constraints that are convexity, orthogonality, conformity and auto-centering. The power diagram of the sites can then be generated.

5.6 Power diagram of the cavity sites

In order to construct the expected transition mesh, the 3D regular triangulation of the cavity sites is generated using an incremental method [10]. The expected power diagram (or more exactly the faces of this one) is obtained by joining the power centers of the tetrahedra belonging to the shell of the same edge (Figure 12).

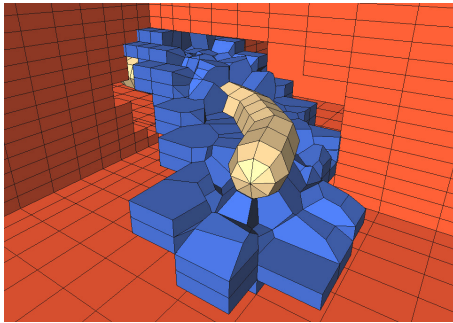
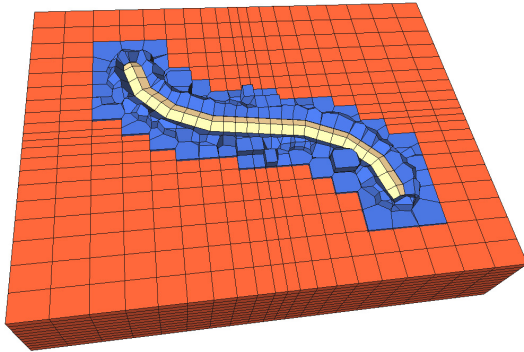


Figure 12: Transition mesh.

5.7 Mesh conformity

At this stage, the generated power diagram is orthogonal, auto-centered and theoretically in conformity with the quadrilaterals of the cavity. Unfortunately, because of numerical imprecisions and because of the presence of some non-co-circular quadrilaterals on the boundary of the deviated wells, this conformity is not guaranteed. It is thus necessary to modify some vertices and some faces of the power diagram in order to ensure the mesh conformity. The algorithm used to solve this problem is based on topological notions and consists in identifying the external face(s) of the transition mesh with the corresponding constrained quadrilateral(s). In particular, if $\mathcal{S}_C = \{S_1, \dots, S_{n_c}\}$ ($4 \leq n_c \leq 8$) is the set of constrained vertices associated with the cell V , V is made in conformity as follows:

- Examine the set of faces of V and determine $\mathcal{P}_F = \{P_1, \dots, P_{n_v}\}$ the set of vertices situated on the external faces of V .
- For each vertex $P \in \mathcal{P}_F$, find the nearest constrained vertex $S \in \mathcal{S}_C$ and replace P by S (Figure 13).

This algorithm is applied to all of the transition cells and the data structure is updated (removal of multiple vertices in the same face and removal of faces whose number of vertices is lower than 3). The resulting transition mesh is then in conformity with the well and the reservoir meshes (Figure 14).

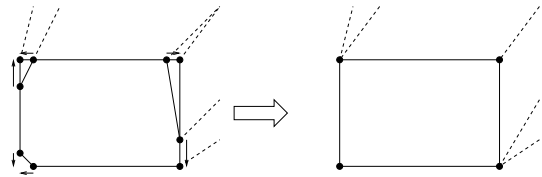


Figure 13: Example of a transition cell made in conformity (removal of 5 vertices and 3 faces).

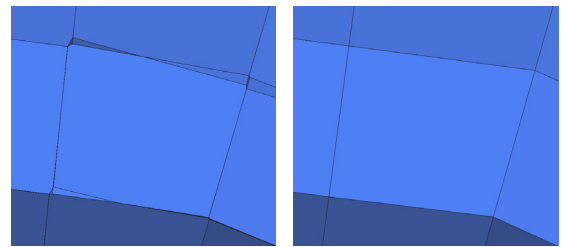


Figure 14: Transition mesh made in conformity.

6. OPTIMIZATION OF THE TRANSITION MESH

Mesh optimization is an operation frequently applied with various objectives and numerous applications. In particular, optimization is interesting because the quality of the numerical solutions (convergence of the numerical schemes, precision of the results) obviously depends on the quality of the computational mesh. For this reason, mesh generation methods are generally completed by an optimization procedure that consists in improving the quality of the mesh. In this section, the quality of a hybrid mesh is introduced as well as an optimization procedure that removes and expands small edges of the transition mesh under quality control and under finite volume properties constraints.

6.1 Definition of quality criteria

The quality or the shape of an element V is a real value measuring its geometrical aspect. Our interest for this quality concept comes from the fact that the solution of a simulation using finite volumes schemes is directly related to the quality of the elements composing the mesh. In fact, in the literature, there are a lot of possible criteria to measure the quality of triangles and tetrahedra but none of them is really adapted to measure the quality of polyhedral cells. Three criteria allowing us to measure the quality of the transition mesh can be defined: a shape quality criterion Q_S , an orthogonality criterion Q_O and a planarity criterion Q_P .

6.1.1 Shape quality criterion

The first quality measure Q_S of a transition cell V is given by:

$$Q_S(V) = \min_{i=1..n_v} \left(\frac{l_i}{h}, \frac{h}{l_i} \right) \quad (7)$$

where l_i is the length of the i^{th} edge of the cell and h is the reference length associated with V which is equal to the average length of the constrained quadrilaterals edges associated with V . This quality measures perfectly the shape or the aspect of an element according to the reference mesh size of the well and the reservoir. It varies from 0, the degenerated cell having a null edge, to 1, the regular polyhedral cell.

6.1.2 Orthogonality criterion

This criterion makes it possible to measure the orthogonality of two adjacent cells by calculating the angle (in degrees) defined by the segment joining the centers of the cells and the plane formed by their shared face. The orthogonality measure Q_O of a face F is

then given by:

$$Q_O(F) = \arcsin \left| \frac{\overrightarrow{P_1 P_2}}{\| \overrightarrow{P_1 P_2} \|} \cdot \vec{n} \right| \times \frac{180}{\pi} \quad (8)$$

where \vec{n} is the normal to F and P_1 and P_2 are the centers of the two adjacent cells located on both sides of F . The orthogonality Q_O varies from 0° , the degenerated face, to 90° , the perfectly orthogonal face. The orthogonality Q_O of a cell V is then defined by the minimal orthogonality of its faces, it is expressed by:

$$Q_O(V) = \min_{F \in V} Q_O(F) \quad (9)$$

6.1.3 Planarity criterion

This criterion, specific to the 3D space, is used to measure the planarity of the faces of the transition mesh. Let F be the face made up of the vertices $\{A_1, \dots, A_{n_v}\}$ and let G be the barycenter of this face. By dividing F into n_v triangles $T_i = (G, A_i, A_{i+1})_{i=1..n_v}$, the planarity measure Q_P (in degrees) of F is given by:

$$Q_P(F) = \max_{i=1..n_v} \arccos |\vec{n} \cdot n_{T_i}| \times \frac{180}{\pi} \quad (10)$$

where \vec{n} is the normal to F and n_{T_i} is the normal to the triangle T_i . The planarity Q_P varies from 0° , the perfectly planar face, to 90° , the crinkled face. The planarity Q_P of a cell V is then defined by the maximal planarity of its faces, it is expressed by:

$$Q_P(V) = \max_{F \in V} Q_P(F) \quad (11)$$

6.2 Optimization

The hybrid mesh construction method generates very small edges and faces which are due to:

- inherent problems related to the method, based on power diagrams which intrinsically can generate very small edges and faces. However this can involve instabilities in numerical simulations and consequently be harmful with the reservoir flow simulations,
- mesh conformity problems related to the presence of constrained quadrilaterals made of non-co-circular vertices.

Considering the fact that small faces are very difficult to eliminate, the optimization procedure consists in removing and expanding small edges of the transition mesh under quality controls (small faces are then removed in an implicit way). Such an optimization decreases the orthogonality and the planarity qualities

of the transition mesh. Three controls are then introduced to validate the modification of an edge under finite volume properties constraints:

- an orthogonality control: a transition cell is said to be orthogonal if its orthogonality Q_O is greater or equal to a given threshold Ω_O (actually $80^\circ \leq \Omega_O \leq 90^\circ$).
- a planarity control: a transition cell is said to be planar if its planarity Q_P is lower or equal to a given threshold Ω_P (actually $0^\circ \leq \Omega_P \leq 10^\circ$).
- an auto-centering control: a cell is said to be auto-centered if its center lie inside this one.

Because of the presence of numerical imprecisions, some transition cells are not initially orthogonal ($Q_O(V) \leq \Omega_O$) and (or) planar ($Q_P(V) \geq \Omega_P$). To take into account these specifications, orthogonality and planarity thresholds are defined for each transition cell. Actually, if a cell V is not initially orthogonal, its orthogonality threshold $\Omega_O(V)$ is equal to its initial orthogonality. Its orthogonality threshold can then improve if the modification of one of its edges improves its orthogonality.

6.2.1 Removal of small edges

Let a and b be the vertices of a small edge. Let \mathcal{B}_a and \mathcal{B}_b be respectively the balls of the vertices a and b and let $\mathcal{B}_{a \cap b}$ be the intersection of \mathcal{B}_a and \mathcal{B}_b .

1st case: a and b are not constrained vertices.

Let $\mathcal{B}_{a \cup b}$ be the union of \mathcal{B}_a and \mathcal{B}_b and let c be the midpoint of the edge $[ab]$: $c = \frac{a+b}{2}$. The edge $[ab]$ is removed and replaced by the vertex c (Figure 15) if and only if the cells of $\mathcal{B}_{a \cup b}$ are orthogonal, the cells of $\mathcal{B}_{a \cup b}$ are planar and the cells of $\mathcal{B}_{a \cap b}$ are auto-centered.

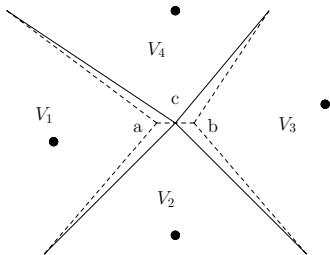


Figure 15: Removal of the edge $[ab]$ when a and b are not constrained vertices.

2nd case: a is a constrained vertex.

The edge $[ab]$ is removed and replaced by the vertex a (Figure 16) if and only if the cells of \mathcal{B}_b are orthogonal,

the cells of \mathcal{B}_b are planar and the cells of $\mathcal{B}_{a \cap b}$ are auto-centered.

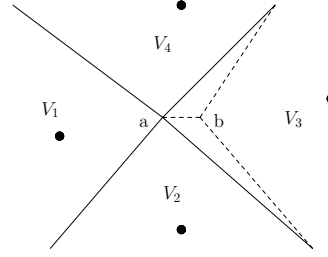


Figure 16: Removal of the edge $[ab]$ when a is a constrained vertex.

6.2.2 Expansion of small edges

When an edge is expanded, all its incident edges are reduced. A control must then be added in order to ensure the improvement of the shape quality of the transition cells which are modified by this expansion.

Let a and b be the vertices of a small edge and let α be a coefficient of expansion such that $1 < \alpha \leq 1.1$. Let \mathcal{B}_a and \mathcal{B}_b be the balls of the vertices a and b .

1st case: a and b are not constrained vertices.

Let $\mathcal{B}_{a \cup b}$ and $\mathcal{B}_{a \Delta b}$ be respectively the union and the symmetrical difference of \mathcal{B}_a and \mathcal{B}_b and let $\tilde{a} = a - \frac{\alpha-1}{2} \overrightarrow{ab}$ and $\tilde{b} = b + \frac{\alpha-1}{2} \overrightarrow{ab}$. The edge $[ab]$ is expanded and replaced by the edge $[\tilde{a}\tilde{b}]$ (Figure 17) if and only if the cells of $\mathcal{B}_{a \cup b}$ are orthogonal, the cells of $\mathcal{B}_{a \cup b}$ are planar, the cells of $\mathcal{B}_{a \Delta b}$ are auto-centered and the average shape quality of the cells of $\mathcal{B}_{a \cup b}$ is better.

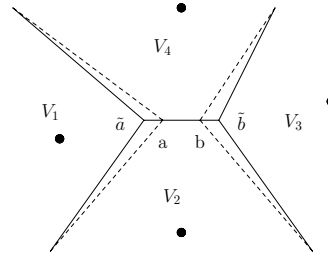


Figure 17: Expansion of the edge $[ab]$ when a and b are not constrained vertices.

2nd case: a is a constrained vertex.

Let \mathcal{B}_{b-a} be the difference of \mathcal{B}_b and \mathcal{B}_a and let $\tilde{b} = b + \frac{\alpha-1}{2} \overrightarrow{ab}$. The edge $[ab]$ is expanded and replaced by the edge $[a\tilde{b}]$ if and only if the cells of \mathcal{B}_b are orthogonal, the cells of \mathcal{B}_b are planar, the cells of \mathcal{B}_{b-a} are auto-centered and the average shape quality of the cells of \mathcal{B}_b is better.

6.2.3 Optimization procedure

Since the modification of an edge degrades the orthogonality and the planarity qualities of the transition cells, the optimization procedure is iterative and consists in modifying in priority very small edges. The procedure is the following:

- In order to eliminate problems due to numerical imprecisions, very small edges whose size is lower than a given threshold Γ_1 (actually $0 < \Gamma_1 \leq 5\%$) are first removed without control.
- Then, edges whose size is lower than a second given threshold Γ_2 (actually $\Gamma_1 \leq \Gamma_2 \leq 40\%$) are removed under finite volume properties constraints.
- Finally, edges whose size is lower than a third given threshold Γ_3 (actually $\Gamma_2 \leq \Gamma_3 \leq 50\%$) are expanded under shape quality control and finite volume properties constraints.

Figure 18 illustrates the removal and the expansion of some edges of the transition mesh.

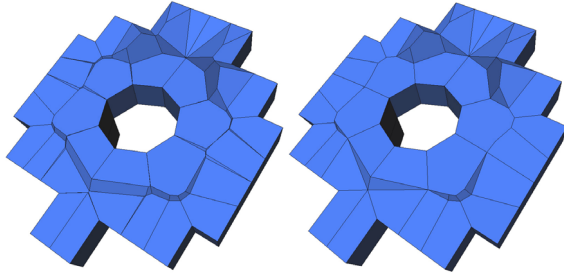


Figure 18: Transition mesh before and after optimization.

7. RESULTS

In this section, some numerical results are presented to show the efficiency of the optimization procedure. In order to have a coherent intention, the tested example is the same as the one presented all along this paper. In order to improve the shape quality of this transition mesh, the orthogonality threshold Ω_O is fixed to 85° and the planarity threshold Ω_P is fixed to 10° . Edges whose size is lower than 5% are first eliminated without control. Then, edges whose size is lower than 30% are removed under finite volume properties constraints. Finally, edges whose size is lower than 40% are expanded under shape quality control and finite volume properties constraints. The results are summarized in Figure 19 and in Table 1 and 2.

	Before optimization	After optimization
Number of vertices	5030	2746
Number of faces	6116	4434
Number of cells	744	744

Table 1: Number of faces and vertices of the transition mesh before and after optimization.

Table 1 shows the number of faces and vertices of the transition mesh before and after the optimization procedure. In this example, 30% of the faces and 45% of the vertices are removed which is significant.

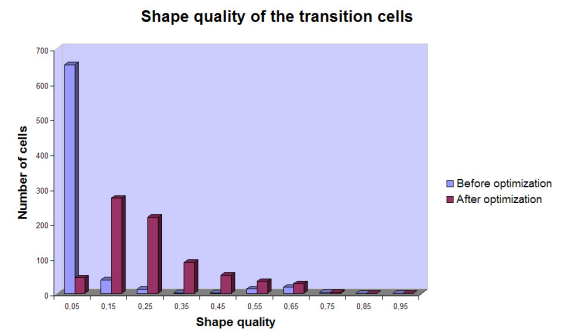


Figure 19: Shape quality evolution of the transition cells.

Figure 19 shows a histogram representing the evolution of the shape quality of the transition cells before and after optimization. While the majority of the transition cells had initially a shape quality contained between 0 and 0.1, they have now a better shape quality contained between 0.1 and 0.4.

	Before optimization	After optimization
Q_S	min.	0.00
	max.	0.71
	average	0.06
Q_O	min.	71.36°
	max.	89.99°
	average	89.78°
Q_P	min.	0.00°
	max.	70.54°
	average	7.05°

Table 2: Qualities evolution of the transition mesh.

Finally, Table 2 shows the minimal, the maximal and the average value of each quality. The proposed method seems to be efficient. The average shape quality was increased from 0.06 to 0.25. While a lot of

degenerated cells were present in the initial transition mesh, only two cells have a planarity which is contained between 10° and 10.56° and do not respect the planarity threshold. These two cells have however a reasonable planarity.

In other respects, the hybrid mesh construction method allows us to insert several wells in the same reservoir mesh. When two or more wells are too close to each other, the corresponding cavities can merge and give rise to only one transition mesh for all these wells. Figure 20 illustrates the case of a hybrid mesh where three radial circular grids around deviated wells are inserted in a non-uniform cartesian reservoir grid. The three radial grids are connected to the reservoir grid by the use of two transition meshes.

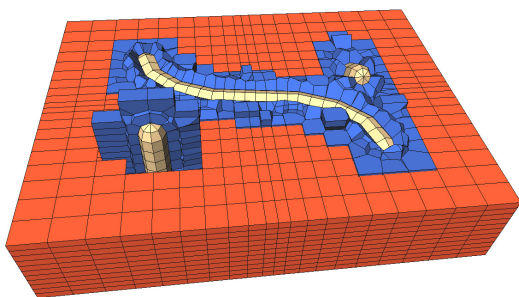


Figure 20: Hybrid mesh composed of one reservoir, three wells and two transition meshes.

8. CONCLUSION

In this paper, a 3D extension of the hybrid mesh proposed in [3] has been presented. The method uses 3D power diagram in order to generate a global conforming mesh between a reservoir, described by a hexahedral cartesian non-uniform grid, and drainage areas around wells, represented by radial circular meshes. Hence, the efficiency of structured grids is kept while accuracy is improved at the drainage areas. Robust and efficient algorithms have been implemented to generate such a transition mesh, taking into account problems of mesh conformity in 3D. In the meantime, some criteria have been introduced to measure the mesh quality, as well as an optimization procedure to remove and to expand small edges of the transition mesh under quality controls and finite volume properties constraints.

The proposed method allows us to take into account cartesian reservoir meshes. However, it can not be applied to real CPG reservoir grids. The future extension consists in considering the geometry of the CPG grids by using anisotropic metrics. This demands to extend all the proposed procedures (in particular the

Delaunay and regular triangulations) to the general anisotropic case.

References

- [1] Balaven S., Bennis C., Boissonnat J., Sarda S. "Generation of Hybrid Grids Using Power Diagrams." *7th International Conference on Numerical Grid Generation in Computational Field Simulations*. 2000
- [2] Flandrin N., Borouchaki H., Bennis C. "Hybrid mesh generation for reservoir flow simulation of new generation: extension to 3D." *ECCOMAS 2004*. Jyväskylä, Finland, 24-28 July 2004
- [3] Balaven S., Bennis C., Boissonnat J., Yvinec M. "Conforming Orthogonal Meshes." *11th International Meshing Roundtable*. Ithaca, New York, USA, september 2002
- [4] Bennis C., Sassi W., Faure J., Chehade F. "One more step in gocad stratigraphic grid generation: Taking into account faults and pinchouts." SPE, editor, *European 3-D Reservoir Modeling Conference*. Stavanger, Norway, 1996
- [5] Aurenhammer F. "Power diagrams: properties, algorithms and applications." *SIAM J. Comput.*, vol. 16, no. 1, 78–96, 1987
- [6] Imai H., Iri M., Murota K. "Voronoi diagrams in the Laguerre geometry and its applications." *SIAM J. Comput.*, vol. 14, no. 1, 69–96, 1985
- [7] Aurenhammer F. "Voronoi diagrams: a survey of a fundamental geometric data structure." *ACM Computing Surveys*, vol. 23, no. 3, 345–405, september 1991
- [8] Fortune S. "Voronoi diagrams and Delaunay triangulations." J.E. Goodman, J. O'Rourke, editors, *Handbook of Discrete and Computational Geometry*, chap. 20, pp. 377–388. CRC Press LLC, 1997
- [9] Watson D.F. "Computing the n-dimensional Delaunay tessalation with application to Voronoi polytopes." *Comp. J.*, vol. 24, pp. 167–172. 1981
- [10] Borouchaki H., Flandrin N., Bennis C. "Diagramme de Laguerre." *C.R. Acad. Sci. Paris*, to appear
- [11] George P., Borouchaki H. *Delaunay triangulation and meshing*. Hermes, 1998
- [12] Borouchaki H., George P., Lo S. "Optimal Delaunay Point Insertion." *IJNME*, vol. 39, 3407–3437, 1996